A summary of the complex dielectric permittivity of ice in the megahertz range and its applications for radar sounding of polar ice sheets

Shuji Fujita*, Takeshi Matsuoka**, Toshihiro Ishida*†, Kenichi Matsuoka*** and Shinji Mae*

*Department of Applied Physics, Faculty of Engineering, Hokkaido University, N13W8, Sapporo 060-8628, JAPAN (†present affiliation: Toshiba Ltd.)
**Communications Research Laboratory, Ministry of posts and telecommunications, 4-2-1 Nukui-kita, Koganei, Tokyo 184-8795, JAPAN
***Institute of Low Temperature Science, Hokkaido University, Sapporo 060-0819, JAPAN

Abstract: Data on the complex dielectric permittivity of ice around megahertz frequencies are reviewed with additions of a few new data sets. Then propagation of electromagnetic waves in the ice sheets is examined. Our purpose is to establish an updated data set to link ice sheet structure (or ice core signals) to radar sounding data. The complex permittivity of ice in the ice sheets is a function of several controlling factors as follows: (1) crystal orientation fabrics, (2) density, (3) impurity concentration (mainly acidity), and (4) temperature. In contrast, both (5) hydrostatic pressure and (6) air-bubble shape have relatively minor effects. The effect of (7) plastic deformation can be significant and needs to be investigated further.

The phase velocity of electromagnetic waves in ice is 168.0~169.5 (m/μs). Present data scatter is about 1 %, probably due to the small dispersion between LF and microwaves, or due to experimental errors in the present data sets. Attenuation is controlled mainly by conductivity arising from the presence of acidity. Because of this dominant acidity effect, the attenuation coefficient is virtually independent of frequency up to several hundred megahertz. As for internal reflections, the three major causes that have been proposed earlier are now conclusive: changes in (1), (2) and (3).

We find the nature of complex reflection coefficients to be as follows. For reflections based on (1) and (2) the amplitude of the complex coefficient is independent of both ice temperature and frequency; the phase delay is virtually zero. In contrast, for reflections based on (3), the amplitude is inversely proportional to frequency, and it is strongly dependent also on temperature. Because the imaginary components are dominant, the phase delay varies between 0.98 and 0.89 (x $\pi/2$ radian). These results suggest that each of the physical factors can be solved quantitatively by analysis of remote sensing data, using frequency and temperature as key parameters.

1. Introduction

In polar ice sheets, mass inputs (snow accumulation) are transported by ice flow to outlet ice streams and glaciers and/or ice shelves. Time scales for this transport can

Physics of Ice Core Records
Edited by T. Hondoh
Hokkaido University Press, 2000, Sapporo

vary up to 10^5 years depending on the physical processes operating within the ice sheets. Therefore understanding of the internal physical processes, internal structure and flow regime is of great importance for understanding past, present, and future changes of the ice sheet. To investigate physical processes operating within the ice sheet and internal structure, ice drilling, ice core analysis, and subsequent borehole logging are direct methods which can provide the most detailed internal information. However, a clear limitation of these direct methods is that the ice coring can never cover a wide area of the vast polar ice sheets.

To investigate the interiors of polar ice sheets, radar sounding techniques have been widely used for several decades, using radar frequencies between a few megahertz and several hundred megahertz [1–3]. A clear and important merit of this remote-sensing technique is that we can investigate a wide area using such platforms as airplanes and ground-based vehicles. We can detect internal structures from internal radio echo layering. Reflections of radio waves from within the ice are caused by sudden changes in complex dielectric properties of ice layers comprising polar ice sheets. Researchers have interpreted the layering as an indicator of constant-time-horizons (or isochrones) for a long time although they did not reach a consensus about mechanisms that caused the changes in the dielectric properties. Since the first report of internal layers in 1964 [2], various mechanism have been suggested and investigated by many researchers for the causes of the sudden changes [3–14]. A history of the findings and earlier interpretations was reviewed by Bogorodskiy et al. [1]. Through all these discussions, the most updated understanding is as follows [13, 15]. (1) There are three major mechanisms for the causes of the sudden changes: changes of density, crystal orientation fabrics, and acidity. (2) Dominant causes of internal reflection change with depth range and with regions in the ice sheet. (3) Whatever the reflection mechanism is, these changes commonly occur along isochrones in the ice sheets. (4) There is a fourth zone in the ice sheet: a basal echo free zone where none of the reflection mechanisms exist. These understandings suggest that radar internal layers are also very important for paleoclimate studies because variations of each factor is closely connected to changes of environment in the past. For example, the variation of ice acidity results from volcanic activity, as well as seasonal and climatic changes in ionic balance in precipitation. Changes in density result from melt features, depth hoar, or precipitation hiatus. Also, origin of the changes in crystal orientation fabrics seems to be changes of chemical components in precipitation [15].

An important application of both ice core data and radar sounding data is that by combining data from these two techniques, we can reconstruct the three dimensional internal structure of the ice sheet. In addition, we can observe by radar sounding how physical processes related to these factors (density, crystal orientation fabrics, acidity, and echo free zone) change in the polar ice sheets [15]. To link between these two kinds of data, an essential physical parameter is the complex dielectric permittivity of ice since it is the controlling factor for radiowave propagation, reflection, and attenuation in ice. Indeed, uncertainty over the dielectric permittivity has made it difficult to interpret the internal reflection mechanisms in the past. Therefore, our

purpose in this paper is to review present knowledge of complex dielectric properties of ice. Based on this knowledge, we will be able to reconstruct a 3-dimensional internal structure in the near-future, probably by an international scientific collaboration. In this paper, we focus on data in the megahertz range, that is, the frequency range applicable to radar sounding of the deep ice sheets. In addition to the examination of earlier data, we present new laboratory data. Conflicts between different laboratory data sets and present limitations are also discussed. Then, wave propagation, attenuation, and reflections in polar ice sheets are discussed.

Ice dielectric properties have been reviewed in several papers. Earlier results have been reviewed by Evans [16], Ray [17], Glen and Paren [18] and Warren [19]. These reviews were written from different points of view but all cover the megahertz range. Dielectric properties of ice containing acidity between LF and microwaves have been discussed by Moore and Fujita [20]. Factors controlling the electrical conductivity of ice from the polar regions were discussed by Wolff et al. [21]. The effect of density has been discussed by Kovacs et al. [22]. Electromechanical phenomena in ice were reviewed by Petrenko [23].

2. Ice dielectric properties

2.1. General description

The relative complex permittivity ε* of ice is described by the Debye expression [18, 24, 25]

$$\varepsilon^* = \varepsilon' - j\varepsilon'' = \varepsilon'_\infty + \frac{\varepsilon'_s - \varepsilon'_\infty}{1 + j\omega\tau} \qquad (1)$$

where ε' is the relative real part, ε" is the imaginary part, ε'_∞ is the relative high-frequency-limit dielectric constant, ε'_s is the relative static dielectric constant, τ is the relaxation time (s), and ω is the angular frequency (radian/s). From equation 1, the real part is

$$\varepsilon'(\omega) = \varepsilon'_\infty + (\varepsilon'_s - \varepsilon'_\infty)\frac{1}{1+\omega^2\tau^2} \qquad (2)$$

and the imaginary part is

$$\varepsilon''(\omega) = (\varepsilon'_s - \varepsilon'_\infty)\frac{\omega\tau}{1+\omega^2\tau^2} \; . \qquad (3)$$

These expressions basically describe the complex permittivity of ice from DC to UHF in the temperature range of the cryosphere. In the microwave region, the component of loss due to lattice vibration starts to be dominant in the imaginary part [26, 27]. The complex conductivity can also be regarded as a complex quantity defined as $\sigma^* = j\omega\varepsilon_0\varepsilon^*$. Thus, the real part of the conductivity is related to the imaginary part of the permittivity as

$$\sigma = 2\pi f \varepsilon_0 \varepsilon'' \; . \qquad (4)$$

An ice Ih crystal has a hexagonal structure which has uniaxial symmetry. Therefore, the complex dielectric permittivity is expressed as a tensor, as follows.

$$\boldsymbol{\varepsilon}^* = \begin{pmatrix} \varepsilon^*_{\perp c} & 0 & 0 \\ 0 & \varepsilon^*_{\perp c} & 0 \\ 0 & 0 & \varepsilon^*_{\parallel c} \end{pmatrix} . \qquad (5)$$

Here, $\varepsilon^*_{\perp c}$ is the component when the

electrical field vector is perpendicular to the c-axis (optic axis); $\varepsilon^*_{\parallel c}$ is the component when the electrical field vector is parallel to the c-axis. Therefore, when polycrystalline ice is isotropic (the c-axes have a randomly distributed orientation) and wavelength is sufficiently larger than the size of crystal grains (as is the case in the megahertz range), then the macroscopic permittivity is

$$\varepsilon^* = \frac{2}{3}\varepsilon^*_{\perp c} + \frac{1}{3}\varepsilon^*_{\parallel c} . \qquad (6)$$

In polar ice sheets, because the crystal orientation fabrics (preferred orientation of c-axis) is generally anisotropic (for example, Budd [28]), the macroscopic permittivity is between the two extreme cases, $\varepsilon^*_{\perp c}$ and $\varepsilon^*_{\parallel c}$. Using the real part, ε', the effective phase velocity of high-frequency electro-magnetic waves is,

$$V_e = \frac{c}{\sqrt{\varepsilon'}} \quad \text{(m/s)}. \qquad (7)$$

2.2. Real part of pure ice

2.2.1. From LF to megahertz range

For static permittivity, ε_s is around 100 (for example, see a textbook [24]). As for the dielectric anisotropy, experimental measurements have been made by a number of workers (for example Humbel et al. [29], Kawada [30], Wörz and Cole [31], Johari and Jones [32] and Johari [33]. Some of them [29, 30] reported that $(\varepsilon^*_{\parallel c} - \varepsilon^*_{\perp c}) / \varepsilon^*_{\parallel c}$ is some 15 %. However, some[31–33] reported that the anisotropy is zero. So far, only research groups who used "zone-refined ice crystals" commonly reported that the anisotropy is zero.

High-frequency limit permittivity (ε'_∞) is around 3.12–3.19 in the temperature range of the cryosphere (see Figure 1) and over a wide frequency range between about 1 MHz and the far-infrared region. It is slightly dependent on both temperature [26, 27, 34, 35] and crystal-orientation [27, 35, 36]. Data in the earlier reviews were scattered within 3.17 ± 0.07 [16, 19]. After Warren's review in 1984, new laboratory data have appeared from several research groups but mainly in the microwave region and not the megahertz range[26, 27, 35–40]. For the real part, recent results tend to agree but there is still uncertainty of about 1 % (Figure 1).

High-frequency limit permittivity (ε'_∞) directly measured at frequencies used for radar sounding (VHF and UHF) was reported by Johari and Charette [41] and by Johari [42]. They measured the complex impedance of a coaxial dielectric cell at frequencies from LF to 100 MHz. Zone-refined single crystals and polycrystalline ice from distilled deionized water were used for the measurements. The tendency of their data is shown in Figure 1. They reported that ice was isotropic with an uncertainty of about 1 %. On the other hand, Westphal [43] carried out dielectric measurement at frequencies between 150 MHz and 2.7 GHz using several Antarctic and Arctic ice samples. An example of the results is shown in Figure 1. The sample is Greenland ice from Tuto Tunnel and contains air bubbles (specific gravity is 0.902 (g/cm^3)). If we correct this result to the value for bubble-free ice, it should be increased by about 1.5 %. This means that it is larger than all other data cited in Figure 1. Unfortunately, for Westphal's data, there is no report about their experimental method, procedure, sample handling or impurity content of the sample. Because of this lack of essential information, we cannot assess these data.

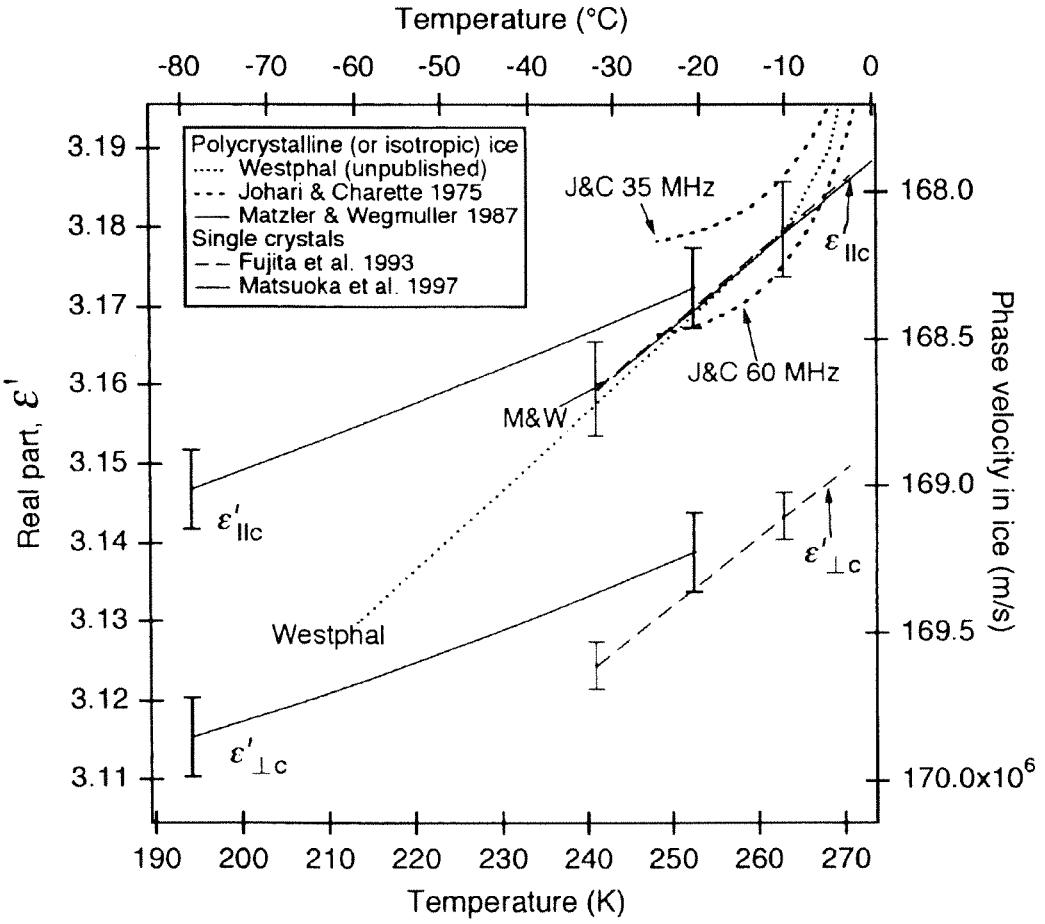

Figure 1: The real part of the permittivity of ice hexagonal crystals in the megahertz range and microwave range. Data are mean values of results in several papers: from Johari et al. [41, 42] using the zone-refined crystal and the polycrystalline ice, from Westphal's unpublished data cited in Jiracek (Tuto tunnel ice with specific gravity 0.902 g/cm^3) [43], from Mätzler and Wegmüller [26] using polycrystalline ice, from Fujita et al. [35] using natural single crystals, and from Matsuoka et al. [37] using natural single crystals. For more details, see the text.

2.2.2. Microwave and Millimeter-wave range

New laboratory data that appeared after Warren's review in 1984 are as follows. Mätzler and Wegmüller [26] measured artificial polycrystalline ice at temperature above about −30 °C and in a frequency range between 2–10 GHz. The method was the cavity resonator method, which is generally suitable to measure the low-loss factor. They reported that the real part can be approximated as a linear function of temperature

$$\varepsilon' = 3.1884 + 9.1 \cdot 10^{-4} \cdot T \qquad (8)$$

where T is temperature in degrees C. The absolute value tends to agree with data in the megahertz range (see Figure 1).

Fujita et al. [35, 36] measured the real part of natural single crystal using a waveguide method at 9.7 GHz. The temperature range was from –30 °C to the melting point. The waveguide methods can provide precise values for the real part by proper calibration whereas it is not suitable for measurement of precise values of imaginary part of the low loss medium (lower than 10^{-3}) in ice. The waveguide method was also used in an earlier measurement by Cumming et al. [44] at 9.4 GHz. Fujita et al. used natural single crystals collected from Mendenhall Glacier. Single crystals from Mendenhall Glacier have been often used in the history of ice physics, and recognized as to be among best ice samples from a viewpoint of impurities and defects [18]. Their measurement showed that ice (at least their natural ice) is birefringent in the microwave region (9.7 GHz). The permit-tivity with the electrical field parallel to the c-axis was larger than the permittivity with the electrical field perpendicular to the c-axis, by about 0.037 (±0.07). Their absolute values of permittivity were lower than those in the megahertz data by about 0.02 (see Figure 1).

Koh [39] measured artificial poly-crystalline ice at 26.5–40 GHz with a free-space method. Temperatures were –2.5 and –15 °C. He reported that the real part was 3.155 (±0.005) at these temperatures and virtually independent of frequency. His result for the absolute value was consistent with Cumming et al. [44] at 9.4 GHz and with that of Fujita et al. [35, 36]. Koh [40] also reported that the real part is 3.17 (±0.05) at 75–110 GHz. This millimeter-wave experiment was carried out using a free space method (transmission method).

Surdyk and Fujita [38] measured a single crystal (Mendenhall Glacier) with the electrical field vector perpendicular to the c-axis at 30–40 GHz at a temperature of –23.5 °C. They used an open resonator method which can provide precise complex values. They reported that the real part was 3.148 (±0.001).

Matsuoka et al. [27, 37] carried out extensive measurements over the wide frequency range between 5 GHz and 39 GHz and at the temperature range between 190–270 K. They used both natural single crystals (from Mendenhall Glacier) and artificially grown polycrystalline ice. Methods were the open resonator method at 30–39 GHz and cavity resonator method at 5 GHz and 10 GHz. The open resonator method is suitable for precise measurement both for the real part and for the imaginary part. By detecting both $\varepsilon'_{\parallel c}$ and $\varepsilon'_{\perp c}$ as two resonance peaks simultaneously from a single crystal, they obtained precise values of dielectric anisotropy (Figure 1). They found that the anisotropy ($\Delta\varepsilon'=\varepsilon'_{\parallel c}-\varepsilon'_{\perp c}$) is 0.0339 (±0.0007) at 252 K. It decreases slightly with decreasing temperature:

$$\Delta\varepsilon'(T) = 0.0256(\pm 0.00137) + 3.57\cdot 10^{-5}\left(6.0\cdot 10^{-6}\right)T \qquad (9)$$

in the temperature range from 190 K to 260 K. Their results from both kinds of resonator (the open resonator and the cavity resonators) were consistent with each other. In addition, they are consistent with the earlier data by Cumming [44], Koh [39], and Fujita et al. [35].

In summary, at microwave and millimeter frequencies, several results [27, 35, 37, 39, 44] are consistent, within experimental error less than about 0.005 (or less than 0.2 % of ε'). Data at 2–10 GHz [26] in Equation (8) are larger by about 0.02.

A data point given by Surdyk and Fujita [38] is larger by about 0.01. It seems that data in the megahertz and microwave regions (lower than 10 GHz) tend to be larger, although megahertz data are very limited. We will discuss the tendency and meaning of this data scatter.

2.2.3. Difference between the zone-refined crystal and the other samples

The present authors carried out a dielectric measurement of single crystal (Mendenhall Glacier) ice at frequencies

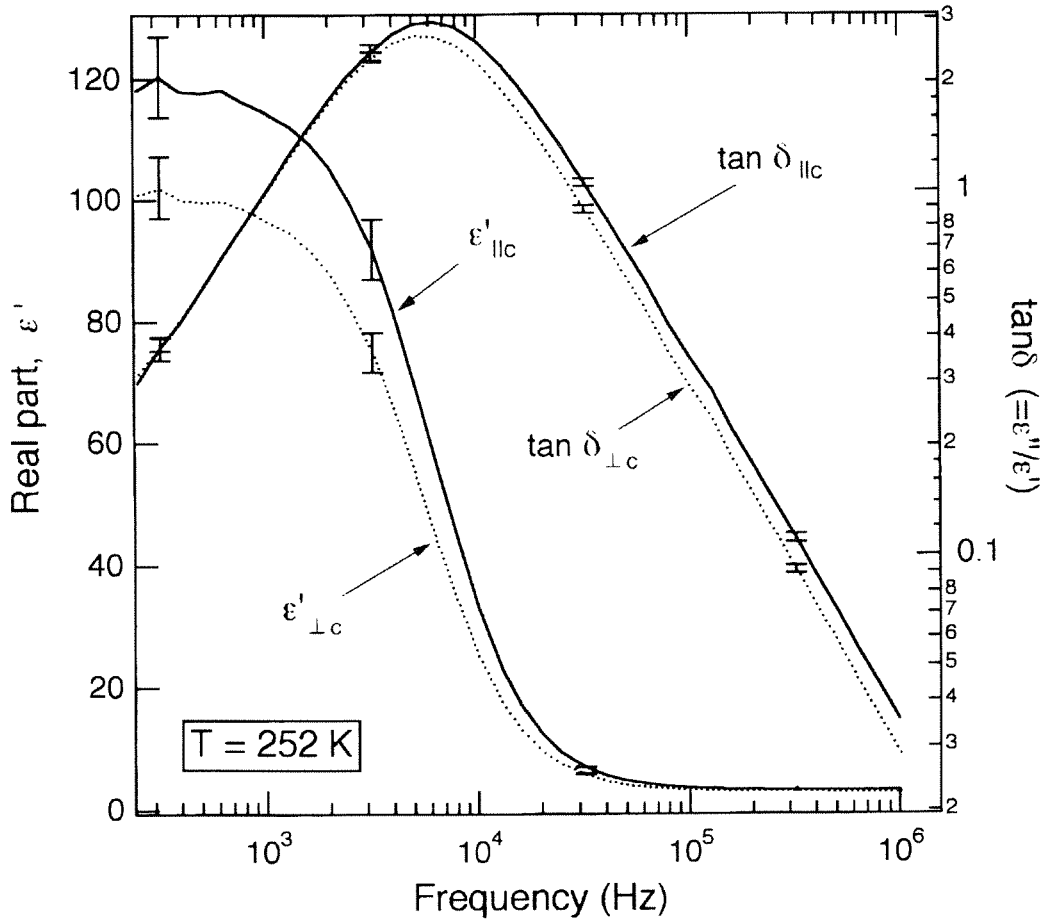

Figure 2: The complex permittivity of a single crystal from Mendenhall Glacier, Alaska. Temperature was 252 K and the frequency range was between 200 Hz and 1 MHz. Two components, the permittivity parallel to the c-axis, $\varepsilon' \parallel c$, and the permittivity perpendicular to the c-axis, $\varepsilon' \perp c$, were independently measured 10 times. Mean values and standard deviations are indicated in the figure. The static permittivity has anisotropy close to 20% ($\varepsilon' \parallel c > \varepsilon' \perp c$). It decreases with increasing frequency to the high-frequency limit value. For the real part at 10^5–10^6 Hz, the figure on an expanded scale is shown in Figure 3. For the loss tangent ($=\varepsilon''/\varepsilon'$), anisotropy was about 20 % ($\tan\delta \parallel c > \tan\delta \perp c$) in the frequency range well above the Debye dispersion. Note that the data of loss tangent contains a systematic error at frequencies lower than about $2 \cdot 10^4$ Hz by a system problem which is not solved yet. Therefore, we cannot assess the relaxation frequencies from the data of loss tangent.

between 200 Hz and 1 MHz in 1994. The results were again in contrast with results from a series of the zone-refined samples [31, 33, 41, 42], which is now quite significant.

The capacitance of disk-shaped ice sandwiched between parallel plate electrodes was measured using an electrode (HP16451B) and precision LCR meter (HP4285A) at a temperature of 252 K. The Mendenhall samples were cut from the bulk and shaped into a cylindrical disk having a c-axis parallel or perpendicular to the c-axis. The orientation of the c-axis, determined using a universal stage, had an error no more than 2–3°. Each type of sample was prepared with 10 mm thickness and 50 mm diameter. Measurements were repeated ten times, changing the thickness up to about 7 mm. Concentration of impurity ion was of the order of 0.1 ppm (mainly Cl^- ions) [36]. A reference measurement using a Teflon sample showed that the real part was 2.070 (±0.003) at 252 K. This value is within a range (2.0–2.1) which generally appears in literature (for example, reference 45). We describe this value in order that we can compare results from various measurements in future.

Figure 2 shows the results (mean values and standard deviations). Static permittivity showed that $\varepsilon'_{\parallel c}$ is clearly larger than $\varepsilon'_{\perp c}$ by about 20 %. This result is consistent with that of Humbel et al. [29] and with Kawada [30]. And it is again in contrast with a series of results for a zone-refined crystal. Our values of $\varepsilon'_{\perp c}$ only agreed with the isotropic component reported by Johari and Jones [32] (permittivity about 100±2 at 252 K). The origin of this contrast is unknown. It can come from the density of lattice defects related to the zone refining.

For the high-frequency limit permittivity, an expanded scale is shown in Figure 3 for the data between 100 kHz and 1 MHz. A result at 1 MHz was preliminarily reported in our earlier paper [37]. Both of the components, $\varepsilon'_{\parallel c}$ and $\varepsilon'_{\perp c}$ decrease with increasing frequency toward the high-frequency-limit values. But anisotropy exists clearly, which is consistent with the microwave data and millimeter wave data [27, 35–37]. Therefore, we can conclude that anisotropy exists over a wide frequency range in the high-frequency-limit permittivity [37]. We can confidently apply these results to polar ice sheets because the anisotropy was detected directly from a deep ice core [46]. In addition, many observational evidences of radiowave birefringence reviewed by Bogorodskiy et al. [1] also support this. The zone-refined ice is a clear exception: birefringence has never be detected except in the optic frequencies.

2.2.4. Frequency dispersion

To understand the effect of frequency, several of the data discussed above are plotted versus frequency in Figure 3. Considering all of the available data, this figure suggests a possibility that the real part decreases with increasing frequency in the megahertz range and in the temperature range of the cryosphere. The total decrease is about 0.04 at 252 K [37]. Applied to radar sounding, it can cause uncertainty in wave velocity of about less than 1 % (see the right axis in Figures 1 and 3). At the moment, we cannot determine whether this data scatter is due to dielectric dispersion or simply due to experimental errors in the laboratory data. Considering the fact that laboratory measurements are difficult in the megahertz range, this property may be found from field measurements using polar ice sheets.

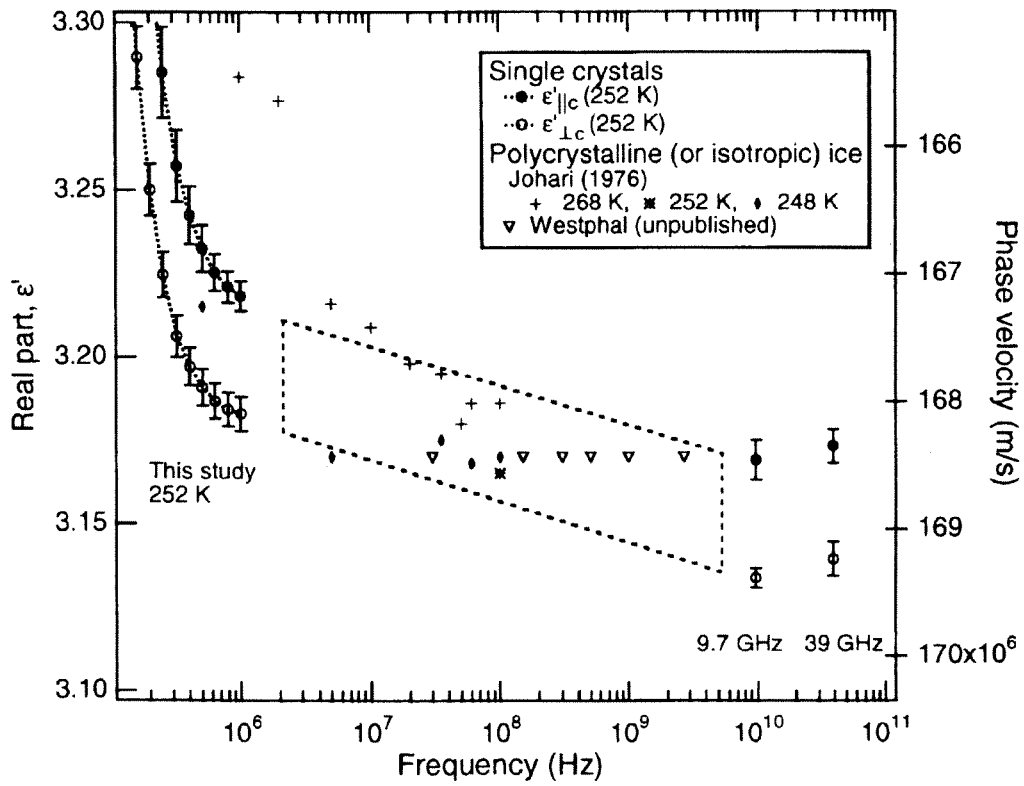

Figure 3: The real part of permittivity from several laboratory measurements versus frequency. Present data scatter implies a possibility that there is a small dispersion in the megahertz range.

2.3. Imaginary part in pure ice

2.3.1. General tendency

At frequencies used for radar sounding, the imaginary part of the permittivity for pure ice is characterized by the high frequency tail of the Debye dispersion and the low frequency tail of lattice vibration in the far-infrared region. As a result, the imaginary part is smallest at frequencies around 1 GHz. Due to the recent progress of dielectric measurement of microwave and millimeter wave [26, 27, 37–39], we have much more knowledge than earlier reviews for the microwave region.

In contrast, as described above, data in the megahertz region are still few. The only available data are from the zone-refined ice [41, 42], at frequencies up to 100 MHz. They are plotted in Figure 4. There are also the unpublished Westphal data [43] in the frequency range between 150 MHz and 2.7 GHz using Antarctic and Arctic Glacial ice. They are also shown in Figure 4.

Under this condition of shortage of real data, an alternative means to derive the imaginary part is interpolation between LF data and microwave data. If the imaginary part is expressed as a summation of Debye dispersion component and lattice vibration component , it is [26, 27]

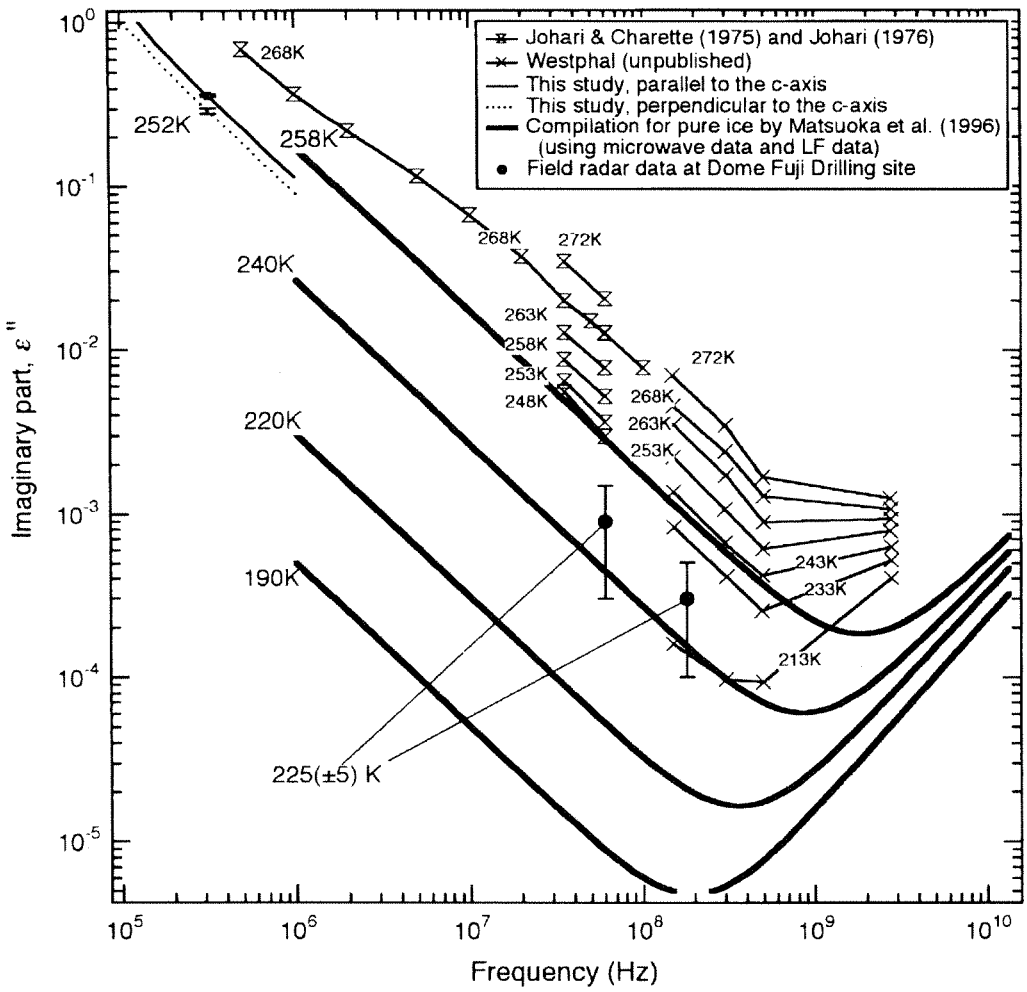

Figure 4: Summary of imaginary part. Matsuoka's data are based on an interpolation between microwave data and LF data [27]. Direct measurements at MHz are few. Johari's data are from artificially grown zone-refined ice. Westphal's data are cited from Jiracek [43], but details of the experimentation are not known. Preliminary results from the field radar experiments at Dome Fuji Station (see text, paper in preparation) are also indicated at two frequencies, 60 MHz and 179 MHz.

$$\varepsilon'' = \frac{A}{f} + Bf^{c} \quad . \tag{10}$$

The first term expresses the Debye component. It is an approximate form of equation (3). The second term expresses the effect of absorption due to lattice vibration. This expression was used earlier by Mätzler and Wegmüller to compile their microwave data at temperatures –5 °C and –15 °C and at frequency between 2 and 90 GHz [26]. Matsuoka et al. [27] updated the parameterization over a wider temperature range between 190 and 265 K. The basic data for the compilation include LF data by Kawada

[30] and microwave data at frequencies between 5 and 39 GHz [27]. Two independent microwave data sets by Mätzler and Wegmüller [26] and Matsuoka et al. [27] are consistent with each other in the microwave region within their experimental error. Matsuoka et al. [27] gave the parameters A, B, and C as in Table 1.

The imaginary part of ice permittivity based on their compilation is shown in Figure 4. It gives much lower values than the megahertz data. This difference between the interpolation (between LF and microwave) and the megahertz data suggests two possibilities. One is (1) megahertz data are basically accurate and an additional component (due possibly to dielectric dispersion or an impurity effect) increased the imaginary part. This is an interpretation proposed by Johari [42]. Another possibility is (2) the megahertz data contain errors and very small values of ice (smaller than 10^{-3}) could not be detected by the investigators. We tend to think that (2) is the case for several reasons given below.

Generally if we use waveguide methods, ordinary parallel-plate electrodes, or impedance measurement of coaxial cells, a detection limit of very small loss factor is of the order of 10^{-2}~10^{-3}, and cannot be smaller even after proper calibrations. If real values of the imaginary part are smaller than this limit, we need to design a resonator system with a quality factor as high as 10^{4}~10^{5}, which is very difficult or unrealistic to design in the megahertz range (in the microwave and millimeter-wave range we can design it). In the paper by Johari [42], no information is provided to justify both their method and the calibration was suitable for measurement of a low loss medium. Walford [47] suggested that radar absorption in a polar ice sheet is proportional to the impurity concentration, on the basis of indirect estimates of the chemistry of some of Westphal's samples. Then, Westphal's data

Table 1: Parameters (A, B, and C) based on interpolation between low frequency (LF) data and microwave data. Data were compiled by Matsuoka et al. [27].

Temperature (K)	A x 10^4	B x 10^5	s.d. x 10^5	C	s.d
190	0.005	1.537	0.391	1.175	0.086
200	0.010	1.747	0.396	1.168	0.077
220	0.031	2.469	0.429	1.129	0.060
240	0.268	3.495	0.468	1.088	0.047
248	0.635	4.006	0.483	1.073	0.043
253	1.059	4.380	0.494	1.062	0.040
258	1.728	4.696	0.500	1.056	0.038
263	2.769	5.277	0.520	1.038	0.036
265	3.326	5.646	0.535	1.024	0.035

from glacial ice and the data from the zone-refined pure ice are difficult to reconcile. All of these conditions imply a possibility that the real value of pure ice is lower.

On the other hand, we carried out radar absorption experiments at the Dome Fuji ice-drilling site (paper in preparation). The electrical conductivity was calculated from 179 MHz and 60 MHz radar profiles using echo strength from the target, an ice-coring drill, in the ice sheet. The result was that the electrical conductivity was approximately 3±2 (μS/m). Using the relation between electrical conductivity and the imaginary part (equation 4), this conductivity gives an imaginary part of about $9(\pm 6)\cdot 10^{-4}$ at 60 MHz and of about $3(\pm 2)\cdot 10^{-4}$ at 179 MHz, respectively. The depth range of the drill was between about 500 m and 1500 m. Temperature of the ice is about 220 K~230 K at these depths [48]. In Figure 4, these values are similar to the values of Johari [42] extrapolated to the Dome Fuji ice temperature. Considering the fact that ice in the inland region of Antarctica contains high level acidity [49] of the order of a few μM, the field measurements of the "impure ice" suggest that the real values of pure ice should be smaller. The amount of electrical conductivity arising from the acidity is discussed below in this paper. Finally, considering the difficulty in laboratory measurements to measure low-loss in this frequency range, it seems that the true value will more likely appear from analysis of the several field measurements than from laboratory experiments.

2.3.2. Anisotropy in the imaginary part

In our experiment using the single crystals (described in 2.2.3.), the imaginary part also showed clear anisotropy. The results are shown in Figures 2 and 4. The imaginary part parallel to the c-axis is larger than that perpendicular to the c-axis by about 20 %. The preliminary result of this experiment at 1 MHz was reported in our earlier paper [37]. This anisotropy is consistent with the anisotropy of static permittivity by about 20 % considering the form of equation 3. This anisotropy was detected only in the high frequency tail of the Debye dispersion. At microwave frequency (the low frequency tail of the far-infrared absorption), anisotropy was not detected within the experimental accuracy [37].

2.4. Complex permittivity arising from the presence of acidity

Changes in electrical properties of ice due to presence of acidity in polar ice sheets have been proposed as one of the main causes of internal reflections by several researchers [10, 12, 14, 15, 48, 50, 51]. The relationship between the electrical conductivity and the chemistry of ice core has been investigated statistically from a vast numbers of ice core data measured using the dielectric profiling technique [21]. Basically this should be the best data to examine polar ice sheets because the data are based on the direct measurements from ice cores. However, the data are in principle the high-frequency limit conductivity measured at LF (below 300 kHz) and at a single temperature. On the other hand, an alternative approach is to investigate doped ice in the laboratory. A possible disadvantage of this approach is that ice properties may not be the same as those of natural ice. Nevertheless, response of the conductivity to acidity is similar between natural ice in the LF range and doped ice in the microwave range [20]. Both data can complimentarily give the estimate of the relationship between the electrical conductivity and the chemistry over a wide

temperature range of the cryosphere and over a wide frequency range used for radar sounding. The complex permittivity of acid-doped ice has been investigated in the microwave range [52, 53] and in the LF range (1 kHz – 30 MHz) [54].

So far, changes in the real part arising from the presence of acidity have not been examined. However, in actual applications (for example to create radargrams based on ice core data) conductivity (or the imaginary part) may not be sufficient. Therefore, to estimate the effect of the real part, one of the present authors (Ishida) investigated the permittivity of acid-doped polycrystalline ice at MHz frequencies.

2.4.1. Real part

The experimental procedure is as follows. The dielectric permittivity of the acid-doped polycrystalline ice was measured at frequencies between 100 MHz and 600 MHz. The temperature range was between −10 °C and −80 °C. Water samples containing strong acids (H_2SO_4, HNO_3, and HCl) were prepared in plastic bags and frozen in a freezer. The sample preparation procedure was the same as that used for our earlier measurement at 9.7 GHz [53]. The experimental method was the transmission method using a coaxial dielectric cell. The experimental setup is schematically shown in Figure 5. The system can detect the real part

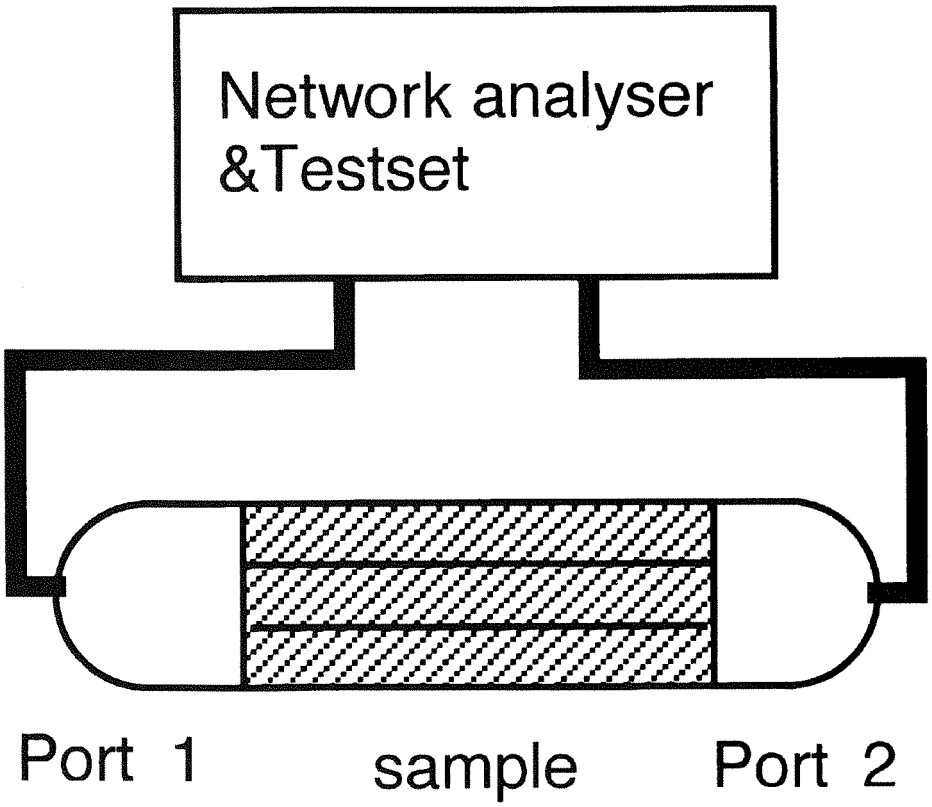

Figure 5: Schematic arrangement of experimental setup for the measurement at megahertz frequencies.

and an imaginary part larger than 10^{-2}. We could detect significant data only for the real part because the imaginary part was far below our detection limit (see the real level of the imaginary part in Figure 4). The Network analyzer was an HP8753C and the S-parameter test set was HP85046A. Samples were shaped into cylindrical rods. Outer diameter, inner diameter, and length were 19.80, 8.65, and 50.0 mm, respectively. Acidity concentrations were between 1.6x 10^{-5} and 4.9x10^{-2} M.

Results were as follows. The real part tended to increase with increasing temperature. It increased also with concentration of acidity in the temperature range above the eutectic points of each acid (H_2SO_4: –73 °C, HNO_3: –43 °C and HCl: –75 °C). An example of relation between acidity and permittivity is shown in Figure 6. We can see that the permittivity increases linearly with the acidity. When acidity is zero, permittivity is between 3.0 and 3.2, which agrees with the high-frequency limit

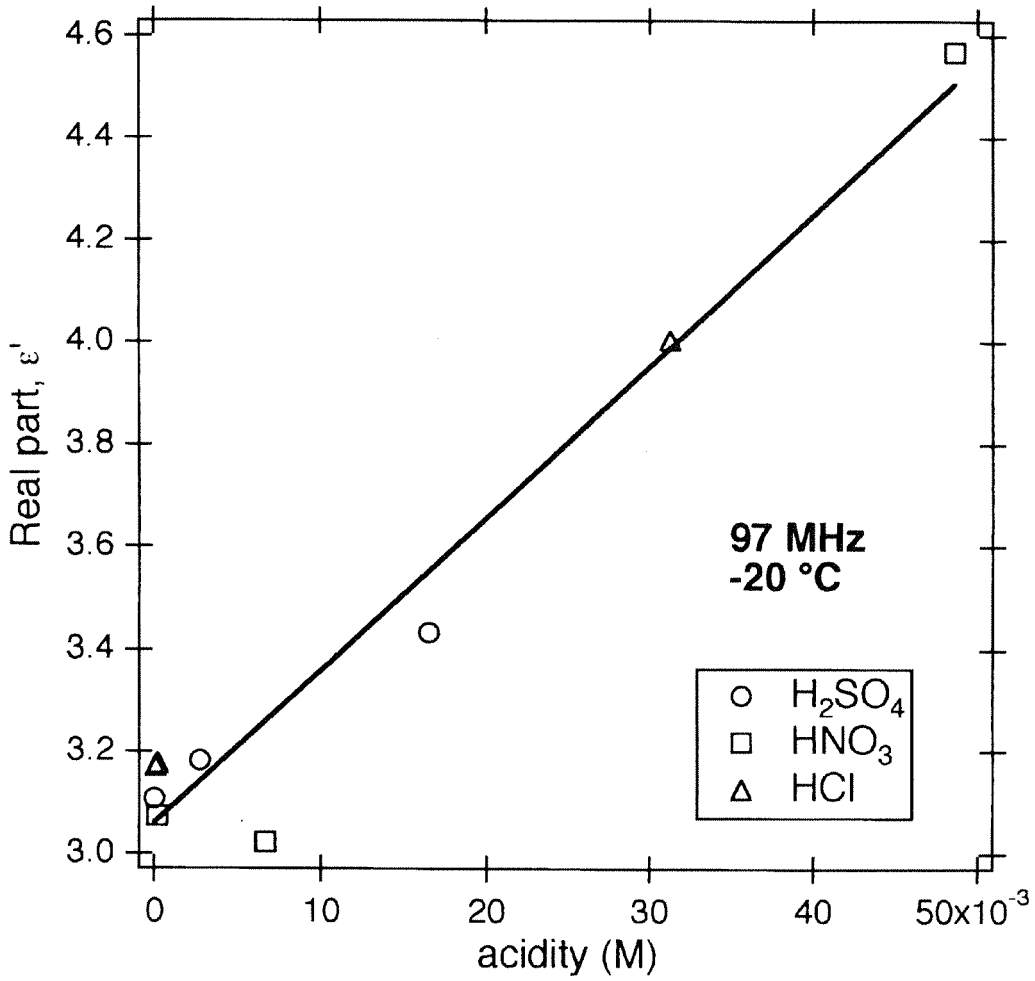

Figure 6: An example of the linear relation between acidity and the permittivity of ice (at –20 °C and at 97 MHz.). Acidity concentrations were between 1.6x10^{-5} and 4.9x10^{-2} M.

permittivity within our experimental error, ±0.1. A similar linear relation was observed in the microwave region (9.7 GHz) [53]. Below the eutectic point for each sample, this linear relation disappears, probably because the liquid phase is frozen below the eutectic points [52]. The real part dropped by about 30 %~50 % at temperatures just below the eutectic points. In the temperature range above –40 °C, we could observe the linear tendency.

The gradient of the linear relation, that is, the permittivity arising from the presence of unit concentration of acidity (hereafter the molar permittivity), was analyzed at several temperatures above –40 °C and over a wide frequency range. The results are shown both in Figure 7 and Table 2. An interesting

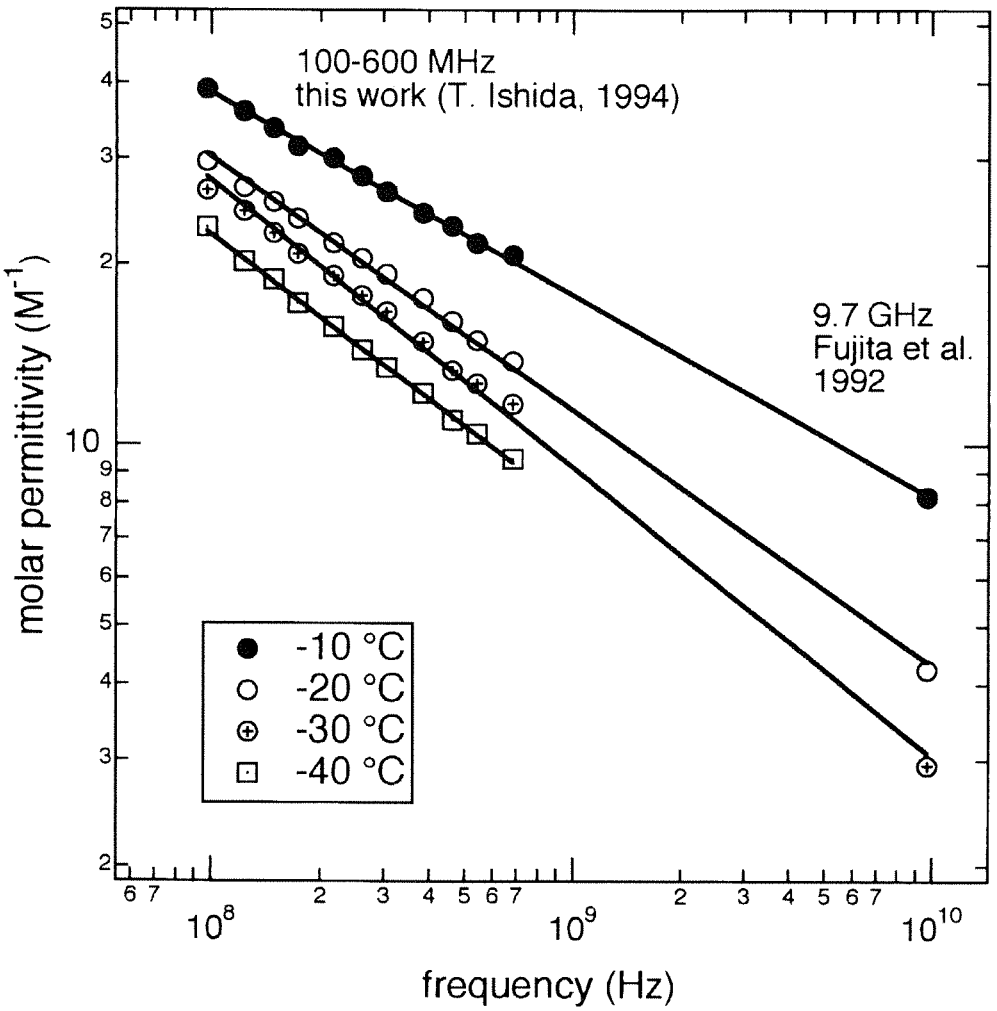

Figure 7: Molar permittivity of acid-doped ice versus frequency. The temperature range was between –10 °C and –40 °C. The frequency range was from 100 MHz and 9.7 GHz. Microwave data (at 9.7 GHz) are from Fujita et al. [53]. The other data are from this study, measured by Ishida. In this frequency range the molar conductivity was approximated by a simple equation 11.

Table 2: Molar permittivity ($d\varepsilon'/dC$) of acid-doped ice at megaherz frequencies.

frequeny (MHz)	temperature −10 °C	−20 °C	−30 °C	−40 °C
97	39.1	29.7	26.7	23.1
123	36.0	26.9	24.6	20.2
148	33.8	25.4	22.6	18.9
173	31.5	23.9	20.9	17.2
217	30.1	21.7	19.2	15.8
261	28.1	20.5	17.8	14.4
306	26.4	19.2	16.7	13.4
384	24.3	17.6	14.9	12.2
463	23.2	16.1	13.3	11.0
541	21.7	15.0	12.7	10.5
680	20.7	13.8	11.6	9.47
9700*	8.22	4.23	2.94	

* Cited from Fujita et al. [53]

feature is that the molar permittivity is approximated by a simple empirical function of frequency at each temperature:

$$\frac{d\varepsilon'}{dC} = 10^{A} \cdot f^{B} \quad . \tag{11}$$

In addition, when the new results in the MHz range are extrapolated to the microwave region, they are in good agreement with the earlier data at 9.7 GHz [53]. This agreement suggests that the molar permittivity is controlled by a consistent mechanism over a wide range of frequency between 100 MHz and 9.7 GHz.

The fitting parameters of equation 11 at 4 temperatures are given in Table 3. This table is useful to estimate increase of permittivity arising from the presence of acidity. We notice that B is generally around −0.3~−0.5. The physical mechanism of this molar permittivity is related to existence of liquid phase in the polycrystalline ice because this effect is observed only above eutectic points. A similar phenomenon was observed in our earlier studies: Matsuoka et

Table 3: Fitting parameters for equation 11.

Temperature (°C)	A	standard deviation	B	standard deviation
−10	4.283	0.024	−0.337	0.002
−20	4.875	0.050	−0.423	0.006
−30	5.279	0.074	−0.480	0.009
−40	4.996	0.043	−0.456	0.005

al. [52] also found sudden changes of molar conductivity (by about 30~50 %) of acid-doped ice at eutectic points. The sudden drop of the permittivity found in this study (30 %~50 %) is almost the same as the sudden drop of the conductivity. Note that changes in permittivity at the eutectic point were not detected by Matsuoka et al. [52]. Because the acidity in their sample was of the order of 10^{-4}, even if some changes happen in permittivity, it should be of the order of 10^{-3}. It is below the detection limit of permittivity (of the order of 10^{-2}).

Figure 8 depicts the frequency dispersion of the molar permittivity, compiled from a series of our experiments [53, 54] including the new data. The temperature was around –20 °C. In the static region (< 10^4 Hz), the molar permittivity is of the order of 10^7. At frequencies between 10^5 Hz and 10^7 Hz, the molar permittivity is inversely proportional to the square of frequency, which may be explained by equation 2. In this case, the relaxation frequency is around 10^4~10^5 Hz, which roughly agrees with the relaxation frequency of the reorientation of the water molecules in the ice lattice. In the frequency range between 10^8 Hz and 10^{10} Hz, the molar permittivity follow equation 11, which

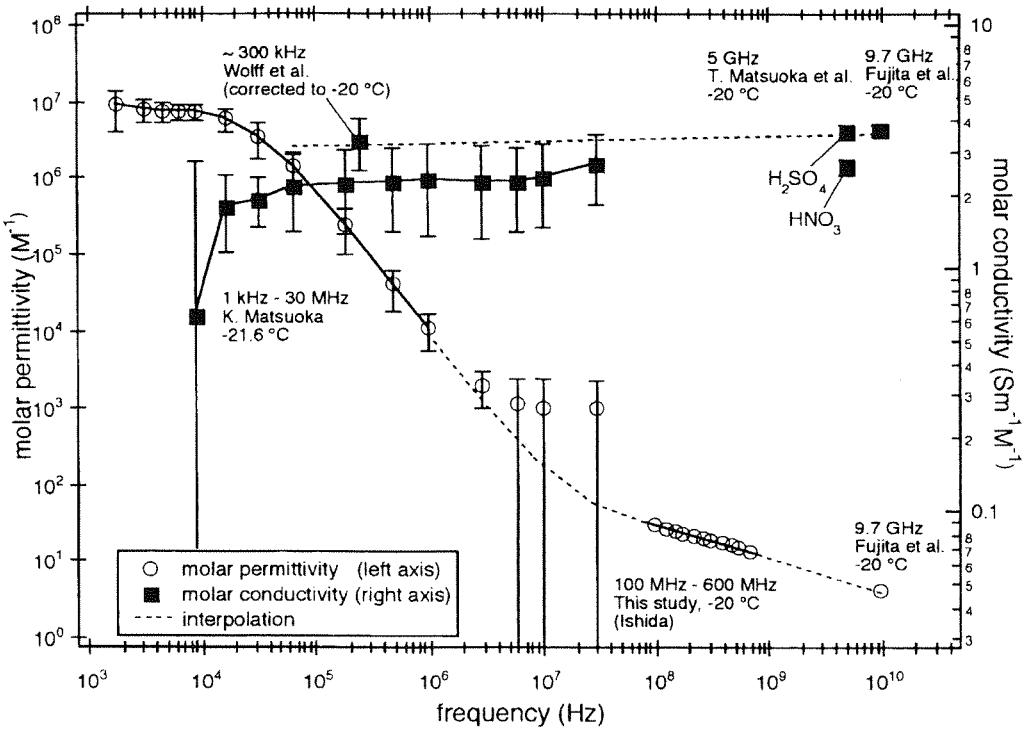

Figure 8: Frequency dispersion of the molar permittivity and molar conductivity of the acid-doped ice, and molar conductivity of ice core counting hydrogen ions. Data source of the doped ice are as follows. The LF data (1 kHz – 30 MHz) are from K. Matsuoka et al. [54]. The megahertz data (100 MHz – 600 MHz) are measured by T. Ishida (this study). The 5 GHz data are from T. Matsuoka et al. [52]. The 9.7 GHz data are from Fujita et al.. Molar conductivity of ice core counting hydrogen ions is from Wolff et al [56] (see text).

suggests that some polarization, different from the reorientation of the water molecules in the ice lattice, takes place in the sample in this frequency range. We interpret that there are a few possible mechanisms that can explain this permittivity arising the presence of the acidity. They are: (1) the reorientation of the water molecules in the liquid phase because liquid water has a relaxation frequency in the microwave range [17], or a kind of space charge polarization caused by the charge due to the reorientation of the water molecules, or (2) dielectric dispersion caused by interfacial polarization, known as the Maxwell-Wagner effect [55]. Both of these two mechanisms can cause the dispersion in the megahertz range. If the first mechanism is the dominant one, it suggest that number of water molecules reorienting in the liquid phase is 10^{-5}~10^{-6} times larger than the number of water molecules reorienting in the ice lattice, considering the static molar permittivity (~10^{7}) and the microwave molar permittivity (~10^{1}) in Figure 8. This interpretation also suggests that the conductivity arising from the reorientation of the water molecules in the liquid phase can change by 10^{-5}~10^{-6} times of the total conductivity by this dispersion.

2.4.2. Conductivity

Changes in the electrical conductivity arising from the presence of acidity was previously discussed by Moore and Fujita [20] for the LF and microwave ranges. They found that response of the conductivity to acidity is similar between natural ice in the LF range and doped ice in the microwave range. After their discussion, several new data sets have been presented: Matsuoka et al. [52] for the microwave range (5 GHz) and concentration of doped acid close to that of actual polar ice, and Matsuoka et al. [54] for the frequency range between 1 kHz and 30 MHz. As for information from the ice core, Wolff et al. [56] gave the molar conductivity derived from the statistical analysis. Figure 8 depicts these data at temperatures around –20 °C. Most of these new data tend to agree with each other within their experimental errors as follows.

For the LF (1 kHz – 30 MHz), the molar conductivity for three strong acids (H_2SO_4, HNO_3, and HCl) is about 2.3±1.0 ($Sm^{-1}M^{-1}$) at –21.6 °C. For the LF (<300 kHz) data from the ice core, Wolff et al. gave the molar conductivity of hydrogen ion as 4(±1) ($Sm^{-1}M^{-1}$) at a temperature of –15 °C. This value was obtained from a statistical analyses using the conductivity and the chemistry of the Greenland ice core. Considering the activation energy they gave (0.22 eV) [56], it is corrected to about 3.3(±0.8) ($Sm^{-1}M^{-1}$) at –20 °C. For the microwave data (9.7 GHz), the molar conductivity for three strong acids (H_2SO_4, HNO_3, and HCl) is about 3.7(±0.2) ($Sm^{-1}M^{-1}$) at –20 °C [53]. The activation energy was 0.19 eV. For the microwave data (5 GHz), the molar conductivity for H_2SO_4 and HNO_3 is about 3.5(±0.2) ($Sm^{-1}M^{-1}$) and 2.4(±0.2) ($Sm^{-1}M^{-1}$) at –20 °C, respectively [52]. The activation energy was 0.16 eV and 0.15 eV, respectively. Several of them tend to agree within their statistical errors, in particular, the LF data from ice core given by Wolff [56], the microwave data by Fujita et al. [53], and the microwave data for the H_2SO_4-doped ice given by Matsuoka et al. [52].

Considering Figure 8 and the results from earlier papers, a summary of our present understanding for ice containing acid impurity is as follows. (1) There is a linear dependence of conductivity on acid concentration for strong acids (H_2SO_4, HNO_3, and HCl) in the temperature range

above the eutectic points. (2) This linear relation is independent of the type of acid [20, 53] or slightly different depending on the type of acid [52]. (3) At the eutectic point of each acid, the conductivity changes by about 30 %–50 % [52], which suggests that liquid phase exist in ice containing acids and that the liquid phase contributes to the total conductivity by this proportion. However, note that this value (30–50 %) is valid only near the eutectic point. (4) The changes in conductivity at the eutectic points have not been detected yet in the natural ice cores. A preliminary experiment by the present authors could not detect it (paper in preparation). (5) Above the eutectic points, the conductivity is well fitted by a simple Arrhenius type equation. (6) There seems to be no evidence of significant dielectric dispersion between LF and microwave [20]. Even if it exist, the changes in the electrical conductivity due to the dispersion is of the order of 10^{-5}~10^{-6} times of the total conductivity (see 2.4.1). (7) Moore and Fujita [20] pointed out that the molar conductivity at LF and at microwaves is well fitted by a model [57] in which concentrated liquid acid at three-grain boundaries form a network, earlier proposed as an explanation for the DC conductivity of polar ice. (8) In case of doped ice, both acid ions and conductivity is localized at grain boundaries and not in the ice lattice (Sugiyama et al. this book). We have no information yet about the localization of conductivity for natural ice cores.

Factors controlling the electrical conductivity from polar regions have been discussed in earlier reviews [18, 21]. Considering these earlier reviews and the summaries of the results described above, it seems that next experiments we need for a better understanding are limited. They are, for example, to investigate localization of conductivity in polar ice cores, and to investigate the relative role of the conductivity in the liquid phase and the conductivity in the ice lattice (probably from point defects). Nevertheless, whatever the conduction mechanism is, a present fact is that the molar conductivity can be determined within a relatively narrow range over a very wide frequency range. We can express it using a simple Arrhenius type equation.

2.5. Effect of the other factors

2.5.1. Effect of density

Effect from density have been discussed for a long time [3, 18, 22]. Robin et al. [3] gave an empirical equation, based on field measurements in Greenland,

$$\varepsilon_r = (1 + 0.851\rho)^2 \tag{12}$$

where ρ is the specific gravity (g/cm^3). If we consider the specific gravity of ice (ρ=0.917), this equation gives permittivity of about 3.17, which agrees with a group of higher values in Figure 1 in the frequency range lower than about 10 GHz. Recently, Kovacs et al. [22] updated the expression as,

$$\varepsilon_r = (1 + 0.845\rho)^2 \ . \tag{13}$$

This equation assumes that the permittivity of ice is about 3.15, which agrees with the most of microwave/millimeter-wave data [35, 37, 39, 44, 54]. Like the small uncertainty in ice permittivity, these expressions also differ from each other by about 0.02.

The effect of density on the imaginary part was investigated for dry snow by Tiuri et al. [58] and for firn by Glen and Paren [18]. In each case, the imaginary part

increases with increasing density. The imaginary part is the maximum when density is maximum (that is, ice). According to Figure 4, it is on the order of 10^{-2} to 10^{-5}. From a view point of application (see later in this paper), the impact of this value both on reflection and attenuation is negligibly small.

2.5.2. Effect of hydrostatic pressure and plastic deformation

There are no laboratory data on the effect of pressure on dielectric constant in the high-frequency-limit range. Johari [59] deduced this from an analysis of the variation of the infrared polarizability with temperature. The value of ε' was anticipated to decrease with pressure at the rate of $96 \cdot 10^{-11}$ Pa^{-1} for H_2O ice. When this value is applied to the real ice sheet, considering that the hydrostatic pressure at a depth of 3000 m is about $27 \cdot 10^6$ Pa [48], the decrease in the permittivity is about 0.026. This value suggests that wave velocity can increase in a very deep ice sheet by no more than 0.5 % (see Figure 1).

As for the effect of plastic deformation, electromechanical phenomena in ice was reviewed by Petrenko [23]. There are no laboratory data in the megahertz range. However, Petrenko pointed out that there are several interesting phenomena that can have some impact on the radiowave propagation. For, dislocations introduced during the process of plastic deformation can generate point defects; they can also capture point defects. These processes can change the charge carrier concentrations, distribution, and its mobility in ice. An example is the experiment performed by Mae and Higashi [60], who found that both concentration and mobility of H_3O^+ ion and OH^- ions are controlled by plastic deformation. At the moment we have no information how these processes interact with ice containing acid impurity. We believe that this topic needs further investigation because this mechanism may explain the recent observational fact that acidity-based internal reflections tend to be weaker or disappear in the high-shear zones in the ice sheet (for example, Plate 2(a) and section 3.2 in Ref. 15). Correct under-standing of these phenomena may open a new possibility for remote sensing of polar ice sheets.

3. Propagation of radio waves

Based on the present knowledge of complex dielectric properties in ice, we will discuss wave propagation and reflections in the polar ice sheet. Wave velocity is approximated as a simple function of the real part (equation (6)). In this section, we focus on two topics: (1) attenuation of radio waves as a function of acid concentration in the polar ice sheet; (2) complex reflection coefficient for internal reflections in the ice sheet.

3.1. Attenuation of radio waves due to conductivity

In the real ice sheet, the ice sheet has background acidity on the order of 1~3 (μM) and peak acidity on the order of 10 (μM). These are very rough numbers that are often found in polar ice cores. Note that they are variable numbers from place to another. We should consider that the peak acidity tend to be smaller in Antarctica and that it can be larger in Greenland [13]. As a result of the acidity, the conductivity arising from the acidity tends to be larger than the conductivity of pure ice. Figure 9 (a–c) shows the conductivity of pure ice, the conductivity arising from the presence of acidity, and total conductivity in ice,

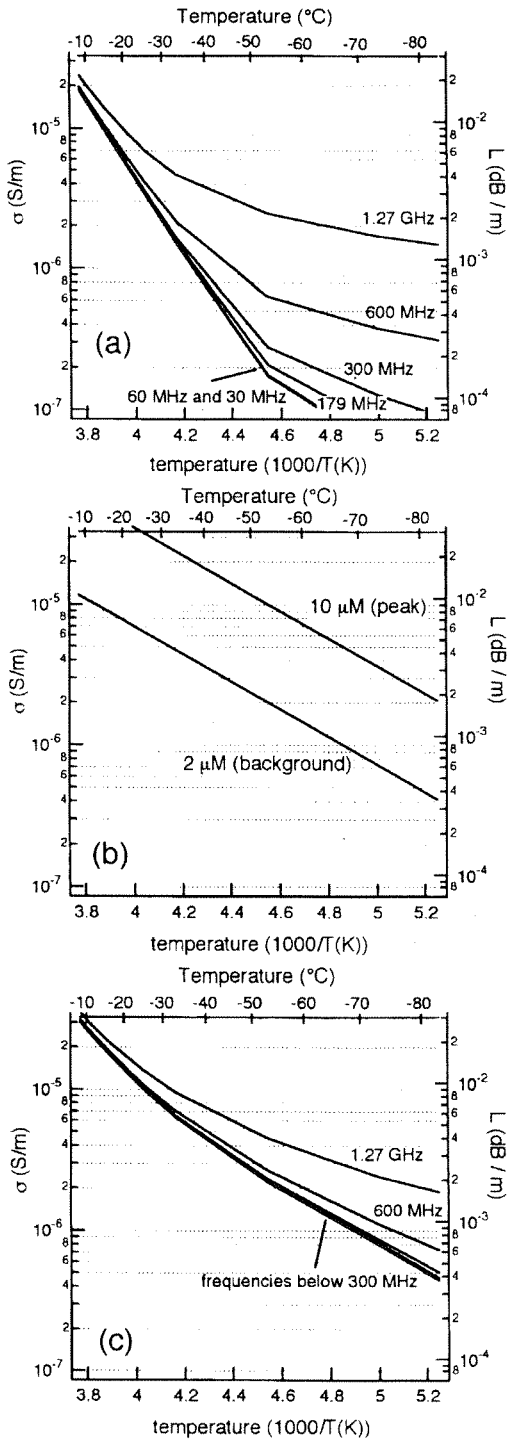

respectively, as a function of frequency and temperature in ice. The absorption loss was also derived as a function of electrical conductivity [1, 61]:

$$L = 8.686\sqrt{\frac{\mu_0}{\varepsilon_0 \varepsilon'}}\frac{\sigma}{2} \quad \text{(dB/m)}. \qquad (14)$$

Here, μ_0 and ε_0 is the magnetic permeability and the dielectric permittivity of free space.

First both the electrical conductivity and the absorption loss were derived for pure ice based on equation (10) and the data in Table 1. The results are shown in Figure 9 (a). This figure means that if the ice is pure, the absorption loss is far below 10^{-2} (dB/m) in the temperature range below –20 °C. This also suggests that the effect of far-infrared lattice vibration appears above about 300 MHz.

Figure 9: The conductivity of the pure ice, the conductivity arising from the presence of acidity, and the summation of both in the ice are estimated for several frequencies used for radar sounding. Also, the absorption loss (L) calculated from the conductivity using equation 14 are indicated. The conductivity is indicated as σ in the left axis in each of the three figures (a), (b), and (c). The absorption loss (L) is indicated by scales in the right axis. Each figure shows as follows. (a) The conductivity of the pure ice. Calculations are based on equation (10) and the data in Table 1. (b) The conductivity arising from the presence of acidity (only). Axis range of this figure is the same as that of Figure 9 (a). For calculation, we assumed that values of background acidity and the peak acidity are roughly 2 μM and 10 μM, respectively. (c) The conductivity in ice containing acids. It was calculated by summing the pure ice component (Figure 9 (a)) and the additional component due to background acidity (2 μM in Figure 9 (b)). The effect of frequency in pure ice (Figure 9 (a)) was obscured by the dominant effect from the increase due to acidity (Figure 9 (b)). This figure suggests that the attenuation of electromagnetic waves is virtually independent of frequency at frequencies below about 600 MHz.

Second, the conductivity arising from the presence of acidity (only) is plotted in Figure 9 (b). In this figure, the scale and axis-range are the same as in Figure 9 (a). For the calculation, a simple Arrhenius type equation was used using the parameters that we discussed in 2.4.2. Figure 9 (b) shows that the conductivity arising from the acidity, on the order of μM, has larger values than the conductivity of the pure ice.

Then, we added this acidity component (the background value in Figure 9 (b)) to the pure ice component (in Figure 9 (a)). The results are plotted in Figure 9 (c). This figure shows that both conductivity and the attenuation coefficients are virtually independent of frequency up to about 600 MHz. For actual radar sounding this implies that the absorption loss is independent of frequency below about 600 MHz. So far, the majority of radar sounders have been designed using frequencies below 100 MHz [1]. However, Figure 9(c) suggests that we can use much wider frequency resources for the radar sounding. In particular, recent studies by Fujita et al. [13, 15] have demonstrated that frequencies above about 100 MHz are now extremely important to detect changes in the crystal orientation fabrics. In addition, when a satellite-borne radar sounder is designed in the future, the frequency should be higher considering the antennae size on the satellite and diffraction of the electromagnetic waves. Indeed, an example of microwave radar sounder was demonstrated by Uratsuka et al. [62], who showed that a radar sounder (1270 MHz, 10 Watt) could detect a bed in the several hundred meter thick ice cap in Ellesmere Island.

3.2. Complex coefficients of internal reflections

Next, we investigate complex reflection coefficients of the internal reflection of the ice sheet. Based on earlier discussions and observations, we derive the complex reflection coefficient due to three factors, changes in crystal orientation fabrics, changes in acidity, and changes in density.

3.2.1. General description of internal reflection coefficients

Quantitative estimation of the reflection coefficients has been carried out in several papers [3, 8–10, 12, 13] using knowledge of dielectric properties available at each time. Because of the recent increase in understanding of dielectric properties of ice as reviewed in this paper, we think that the time has come to assess the full complex component of the reflection coefficient for each mechanism. Preliminary comparison between crystal-orientation-based reflections and acidity-based reflections were performed by Fujita and Mae [13]. We improve this by introducing the full complex component and density-based reflections.

The reflection coefficient is calculated, following Ackley and Keliher [9] and Moore [12]. The characteristic bulk impedance Z_i of layer i is defined by

$$Z_i = \frac{j\mu_0\omega}{\gamma_i} \tag{15}$$

where γ_i is the propagation constant:

$$\gamma_i^2 = \varepsilon_0\mu_0\varepsilon_i\omega^2 + j\mu_0\sigma_i\omega \tag{16}$$

where ε_i and σ_i are the relative permittivity and conductivity of the layer, respectively.

The reflection amplitude r_i^* (it is $r\cdot\exp(i\theta)$ in polar coordinates. r is the

amplitude, θ is the phase delay) at a boundary within the medium is, when the changes in impedance between layer is small,

$$r_i^* \approx \frac{Z_{i-1} - Z_i}{Z_{i-1} + Z_i} . \quad (17)$$

3.2.2. Acidity-based reflections

Acidity-based reflections were calculated based on equation (11) (the molar permittivity) and the molar conductivity expressed by an Arrhenius equation. Because the acidity peaks in ice cores are of the order of 10 μM, we used this concentration for our estimation. In actual ice sheets, it can be lower. But in some extreme cases it can be also about 20~30 μM. Calculated results are shown in Figure 10. The amplitude is virtually inversely proportional to frequency, as derived in earlier studies [12, 13]. The coefficients are dominated by the imaginary parts, which

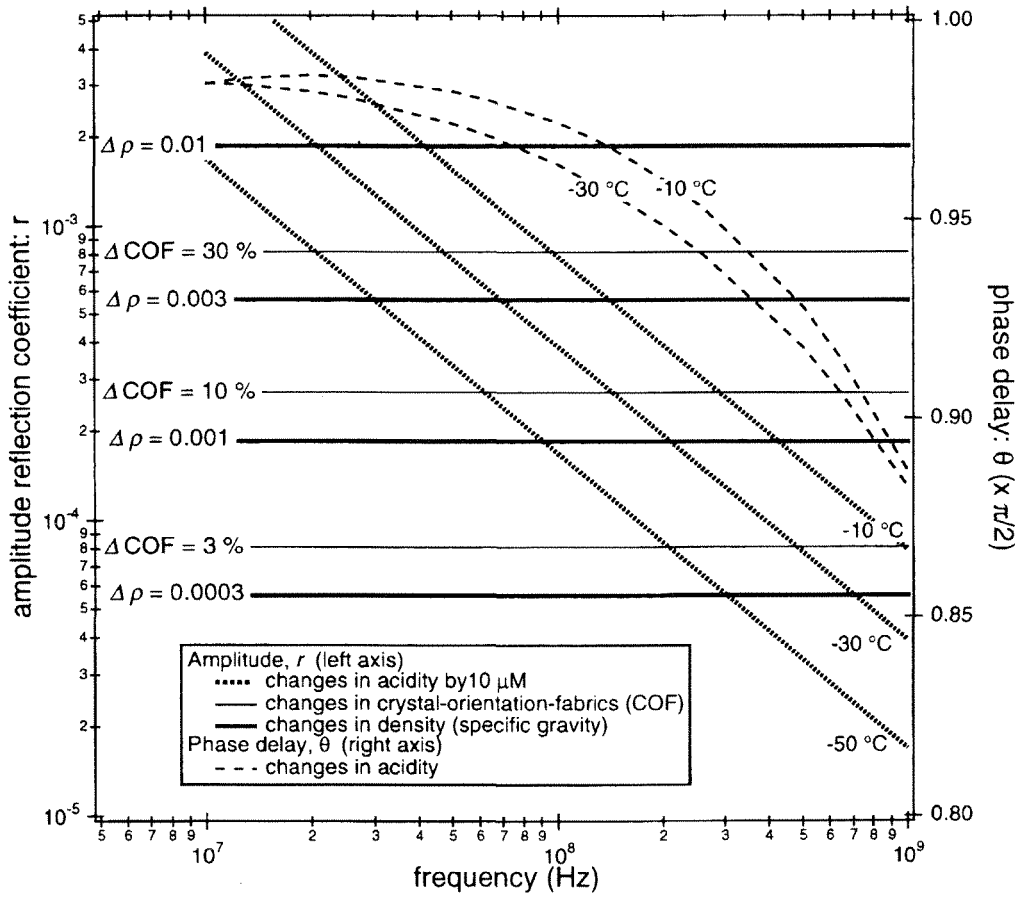

Figure 10: A relation between the complex reflection coefficients ($r^* = r \cdot \exp(i\theta)$) and changes in the complex permittivity in the ice sheet. Calculations are carried out for the three major causes: changes in crystal orientation fabrics, changes in acidity, and changes in density. For reflections due to changes in acidity, the phase delay (right axis) is close to $\pi/2$. But it decreases with increasing frequency. For changes in the crystal orientation fabrics and changes in density, the phase delay is virtually zero.

causes phase delays by angles close to $\pi/2$. However, because the real parts are significant as we discussed in 2.4.1, the phase delay (θ) tends to decrease from $0.98 \cdot \pi/2$ to $0.89 \cdot \pi/2$ with increasing frequency (see the right axis in Figure 10). Because the conductivity arising from the presence of acidity follows the Arrhenius equation, r is smaller when ice temperature is lower. This result suggests that the nature of the acidity-based reflections is as follows. (1) Acidity-based reflections are more dominant when ice temperature is higher and the frequency used for radar sounding is lower. (2) For exact calculations to reconstruct radargrams based on ice-core records, we need to take account of the real part and the phase delay.

3.2.3. Crystal orientation fabrics

We assume that due to changes in crystal orientation fabrics the dielectric permittivity tensor can change easily by about 10 % of the dielectric anisotropy (see Fujita and Mae [13]). In fact, discontinuous fluctuations of the crystal orientation fabrics were detected in the 2504-m ice core from Dome Fuji (N. Azuma, personal communication 1998). He found that the cluster strength of the single maximum pattern fluctuates dramatically even in a 1-m portion of the ice core. Normally, if thickness of fluctuations are more than several centimeters, it is sufficiently thick to produce strong reflections even if we consider interference effect (for example, see Figures 3 and 4 in [13]). As input data, contributions of dielectric anisotropy of 30 %, 10 %, and 3 % were used. Results are shown in Figure 10. r is virtually independent of both frequency used for radar sounding and temperature in the ice. Because less than 20 % (the imaginary part of the dielectric anisotropy (see 2.3.2 and Figure 4)) of the imaginary part contributes to the changes in the imaginary part due to changes in crystal orientation fabrics, the phase delay (θ) is always less than 0.01 radian, which is negligibly small. Therefore, we conclude that changes in imaginary part due to changes in crystal orientation fabrics have virtually no effect on reflection.

3.2.4. Density

As input data, we used changes in specific gravity of 0.01~0.0003 (g/cm^3) (that is, density fluctuation is about 1 % ~ 0.03% of ice). Results are shown in Figure 10. Like the reflections due to changes in crystal orientation fabric, r is virtually independent of both frequency used for radar sounding and temperature in the ice. Because less than 1 % of the imaginary part (in Figure 4) contributes to the imaginary part, the phase delay due to the imaginary part is always less than 0.001 radian, again negligibly small. Therefore we can again conclude that the imaginary part has no effect on this reflection mechanism.

3.2.5. Comparison

Exact estimation based on the updated complex data set was established in Figure 10. These data are essential for precise analysis of the radar data at megahertz frequencies. The results justify our earlier comparison between acidity-based reflections and crystal-orientation-based reflections [13] but gave exact values including the phase delay and the comparison with the density-based reflections. The changes in acidity cause reflections basically due to changes in the imaginary part. Amplitude reflection coefficient decreases inversely proportional to frequency. It is strongly dependent also on temperature. In contrast, changes in crystal orientation fabrics or density give changes only in the real part. Therefore no phase delay appears in the

reflection coefficients. The coefficient is independent of both frequency used for radar sounding and temperature in ice. These results affirm that we can detect these parameters using a multi-frequency radar sounding technique [13, 15]. In particular, frequencies above 100 MHz are very useful to detect changes in crystal orientation in the ice sheet because the acidity-based reflection is weaker. When we create radargrams based on ice core data, change in the real part due to change in acidity is a factor to be taken into account.

We briefly examine another proposed mechanism, change in shape of air bubbles with depth. Ackley and Keliher [9] estimated the possible magnitude of reflection from elongated air bubbles. According to their estimation, reflection coefficients (r) are lower than about 10^{-4} (or about −80 dB) when the ratio between the long axis and the short axis is about 10. This value is small compared with the three major mechanisms in Figure 10. It is a clear fact that density-based reflections are strongly dominant in the depth range where air bubbles can exist. Moreover, it is not realistic that air bubbles in inland of ice sheets have such extremely elongated air bubbles. Considering these conditions, the bubble-shape-factor cannot be a major cause of internal reflections.

Finally, we mention the basal echo free zone (EFZ) found in the Antarctic ice sheet. The examples have been reported in a few papers [11, 15, 63]. The EFZ is several hundred meters thick. An important implication of this zone is that there is not any reflection mechanisms that we have discussed above. Present understanding was discussed by Fujita and others (1999): the EFZ seems more likely a stagnant ice composed of recrystallized ice, than a high shear zone. Since the physical conditions near the ice-sheet base are very important and since it is a difficult task to get ice samples, the EFZ should be extensively investigated by radar sounding.

Conclusions

Data on the complex dielectric permittivity of ice around megahertz frequencies are summarized with addition of some previously unpublished data. Then, propagation of radio waves in ice sheets is examined. The complex permittivity of ice in the cryosphere is a function of several controlling factors: (1) crystal orientation fabrics, (2) density, (3) acidity concentration, and (4) temperature. In contrast, both (5) hydrostatic pressure and (6) air-bubble shape have little effects. The effect of (7) plastic deformation seems to be significant and needs further investigation. In particular, a possible interaction between plastic deformation and the complex permittivity arising from the presence of acidity should be studied. In addition, further experiments are necessary for a better understanding of factors controlling the electrical conductivity from polar regions. Considering the present knowledge described in this paper, it seems that next experiments we need are, for example, to investigate localization of conductivity in polar ice cores, and to investigate the relative role of the conductivity in the liquid phase and the conductivity in the ice lattice. Whatever the conduction mechanism is, a present fact is that the molar conductivity can be determined within a relatively narrow range over a very wide frequency range using a simple Arrhenius type equation.

The phase velocity of radio waves in ice is 168.0~169.5 (m/μs). Present data scatter

is about 1 %, possibly due to the small dispersion between LF and microwave regions, or due to experimental errors. To remove this uncertainty, a realistic method for experiment is field radar measurements, rather than laboratory measurements. We suggest that the imaginary part of the pure ice is lower than results indicated by a small amount of old laboratory data, considering the values at surrounding frequencies and the results of field measurements. This point should also be confirmed by additional field measurements. Attenuation in the ice sheets is controlled mainly by conductivity arising from the presence of acidity. Because of this dominant acidity component, the attenuation coefficient is virtually independent of frequency over a frequency range up to several hundred (about 600) megahertz. This result suggests that the absorption loss is unchanged even if we use frequencies higher than 100 MHz, which is an important frequency range for investigation of crystal orientation fabrics and for the future satellite-borne radar sounder.

As for internal reflections, we affirmed that the three major causes that had been proposed earlier are conclusive, changes in crystal orientation fabrics, changes in acidity, changes in density. For reflections based on crystal orientation fabrics and density, the amplitude of the complex coefficient is independent of both ice temperature and frequency used for radar, and the phase delay is virtually zero. In contrast, for reflections based on changes in acidity, the amplitude is inversely proportional to frequency, and it is strongly dependent also on temperature. Because the imaginary components are much more dominant than the real part, the phase delay varies between $0.98 \cdot \pi/2$ and $0.89 \cdot \pi/2$ (radian). These results suggest that each of the physical factors can be solved quantitatively by analysis of radar sounding data, using frequency and temperature as key parameters.

References

1. Bogorodskiy, V.V., Bentley, C.R. and Gudmandsen, P.E. *Radioglaciology* (D. Reidel, Norwell, Mass, 1985).
2. Bailey, J.T., Evans, S. and Robin, G. de Q. *Nature* 204, 420-421 (1964).
3. Robin, G. de Q., Evans, S. and Bailey, J.T. *Phil. Trans. Roy. Soc. London, Ser. A* 265, 437-505 (1969).
4. Harrison, C.H. *J. Glaciol.* 12, 383-397 (1973).
5. Robin, G. de Q. *J. Glaciol.* 15, 49-64 (1975).
6. Gudmandsen, P. *J. Glaciol.* 15, 95-101 (1975).
7. Paren, J.G. and Robin, G. de Q. *J. Glaciol.* 14, 251-259 (1975).
8. Clough, J.W. *J. Glaciol.* 18, 3-14 (1977).
9. Ackley, S.F. and Keliher, T.E. *J. Geophys. Res.* 84, 5675-5680 (1979).
10. Millar, D.H.M. *Nature* 292, 441-443 (1981).
11. Robin, G. de Q. and Millar, D.H.M. *Ann. Glaciol.* 3, 290-294 (1982).
12. Moore, J.C. *Ann. Glaciol.* 11, 95-99 (1988).
13. Fujita, S. and Mae, S. *Ann. Glaciol.* 20, 80-86 (1994).
14. Miners, W.D., et al. *J. Phys. Chem.* B 101, 6201-6204 (1997).
15. Fujita, S., et al. *J. Geophys. Res.*, 104(B6), 13013-13024 (1999).
16. Evans, S. *J. Glaciol.* 5, 773-792 (1965).
17. Ray, P.S. *Appl. Opt.* 11, 1836-1844 (1972).

18. Glen, J.W. and Paren, J.G. *J. Glaciol.* 15, 15-38 (1975).
19. Warren, S.G. *Appl. Optics* 23, 1206-1225 (1984).
20. Moore, J.C. and Fujita, S. *J. Geophys. Res.* 98, 9769-9780 (1993).
21. Wolff, E.W., Miners, W.D., Moore, J.C. and Paren, J.G. *J. Phys. Chem.* B. 101, 6090-6094 (1997).
22. Kovacs, A., Gow, A.J. and Morey, R.M. *Cold Regions Science Technology* 23, 245-256 (1995).
23. Petrenko, V.F. *CRREL Special Report* Vol. 96, No. 2, 30 (1996).
24. Fletcher, N.H. *The Chemical Physics of Ice* (Cambridge University Press, Cambridge, 1970).
25. Petrenko, V.F. *CRREL Special Report* Vol. 93, No. 20 (1993).
26. Mätzler, C. and Wegmüller, U. *J. Phys. Appl. Phys.* 20, 1623-1630 (1987).
27. Matsuoka, T., Fujita, S. and Mae, S. *J. Appl. Phys.* 80, 5884-5890 (1996).
28. Budd, W.F. *Zeitschr. Gletscherkunde Glazialgeol.* 8, 65-105 (1972).
29. Humbel, H., Jona, F. and Scherrer, P. *Helv. Phys. Acta.* 26, 17-32 (1953).
30. Kawada, S. *J. Phys. Soc. Jpn.* 44, 1881-1886 (1978).
31. Wörz, O. and Cole, R.H. *J. Chem. Phys.* 51, 1546 (1969).
32. Johari, G.P. and Jones, S.J. *J. Glaciol.* 21, 259-276 (1978).
33. Johari, G.P. *Contemporary Phys.* 22, 613-642 (1981).
34. Gough, S.R. and Davidson, D.W. *J. Chem. Phys.* 52, 5442-5449 (1970).
35. Fujita, S., Mae, S. and Matsuoka, T. *Ann. Glaciol.* 17, 276-280 (1993).
36. Fujita, S., Shiraishi, M. and Mae, S. *The proceedings of the International Symposium on the Physics and Chemistry of Ice* (Editors: Maeno, N. and Hondoh, T.) , 415-421 (1992).
37. Matsuoka, T., Fujita, S., Morishima, S. and Mae, S. *J. Appl. Phys.* 81, 2344-2348 (1997).
38. Surdyk, S. and Fujita, S. *Geophys. Res. Lett.* 22, 965-968 (1995).
39. Koh, G. *J. Appl. Phys.* 71, 5199-5122 (1992).
40. Koh, G. *Geophys. Res. Lett.* 24, 2311-2313 (1997).
41. Johari, G.P. and Charette, P.A. *J. Glaciol.* 14, 293-303 (1975).
42. Johari, G.P. *J. Chem. Phys* 64, 3998-4005 (1976).
43. Jiracek, G.R. *The University of Wisconsin, Geophysical & Polar Research Center, Research Series* 67-1 , 10-17 (1967).
44. Cumming, W.A. *J. Appl. Phys.* 23, 768-773 (1952).
45. Hippel, A. *Dielectric materials and applications* 1-134-144 (The technology press of M.I.T. and John Wiley & Sons, Inc., New York and London, 1954).
46. Matsuoka, T., Mae, S., Fukazawa, H., Fujita, S. and Watanabe, O. *Geophys. Res. Lett.* 25, 1573-1576 (1998).
47. Walford, M.E.R. *J. Glaciol.* 7, 89-94 (1968).
48. Fujita, S., et al. *Memories of National Institute of Polar Research, Special Issue* No.49 (Ice Drilling Technology; Proceedings of the Fourth International Workshop on Ice Drilling Technology (Tokyo, April 20-23, 1993)) , 347-357 (1994).
49. Kamiyama, K., Fujii, Y., Watanabe, O. and Yamada, T. *Antarctic Record* 34, 119-129 (1990).
50. Hammer, C.U. *J. Glaciol.* 25, 359-372 (1980).
51. Millar, D.H.M. *Ann. Glaciol.* 3, 199-203 (1982).

52. Matsuoka, T., Fujita, S. and Mae, S. *The J. Phys. Chem. B* 101, 6219-6222 (1997).
53. Fujita, S., Shiraishi, M. and Mae, S. *IEEE Transactions on Geoscience and Remote Sensing.* 30, 799-803 (1992).
54. Matsuoka, K., et al. *Proc. NIPR Symp. Polar Meteorol. Glaciol.* 10, 25-35 (1996).
55. Hasted, J.B. *Aqueous Dielectrics* 1-302 (Chapman and Hall Ltd., London, 1973).
56. Wolff, E.W., et al. *J. Geophys. Res.* 100, 16249-16264 (1995).
57. Wolff, E.W. and Paren, J.G. *J. Geophys. Res.* 89, 9433-9438 (1984).
58. Tiuri, M.E., Sihvola, A.H., Nyfors, E.G. and Hallikainen, M.T. *IEEE J. Oceanic Eng.* oe-9, 377-382 (1984).
59. Johari, G.P., Chew, H.A.M. and Sivakumar, T.C. *J. Chem. Phys.* 80, 5163-5169 (1984).
60. Mae, S. and Higashi, A. *Crystal Lattice Defects* 4, 295-308 (1973).
61. Sander, K.F. and Reed, G.A.L. *Transmission and propagation of electromagnetic waves.* 1-458 (Cambridge University Press, Cambridge, 1986).
62. Uratsuka, S., et al. *Memories of National Institute of Polar Research, Special Issue* (Proceedings of the Fourth International Symposium on Environmental Research in the Arctic (Tokyo, July 19-21, 1995) 49, 387-394 (1996).
63. Robin, G. de Q., Drewry, D.J. and Meldrum, D.T. *Phil. Trans. Roy. Soc. London, Ser. B* 279, 185-196 (1977).